EurJOC European Journal of Organic Chemistry

FULL PAPER

DOI: 10.1002/ejoc.201500552

Low-Energy-Gap Organic Based Acceptor–Donor–Acceptor π-Conjugated Small Molecules for Bulk-Heterojunction Organic Solar Cells

Edison Castro,[a] Andrea Cabrera-Espinoza,[a] Eva Deemer,[b] and Luis Echegoyen*[a]

Keywords: Energy conversion / Solar cells / Organic photovoltaics / Small molecules

We describe the detailed syntheses and characterization of two new electron-donor molecules based on an acceptor–donor–acceptor (A–D–A) structure with carbazole as the electron-rich building block, benzothiadiazole (BT) as the electron-acceptor building block and octylrhodanine as the end group. We also examined the effects of a thiophene group as a spacer between the BT and the carbazole units on the optoelectronic, morphological and photovoltaic properties. The presence of the thiophenes has pronounced effects on both the optical and electrical properties. **ECTBT**, which contains thiophenes units, showed a red-shifted absorption and a lower HOMO level compared to **ECBT**, which has no thiophene spacers. Optimized photovoltaic device fabrication based on **ECTBT** and [6,6]-phenyl-C_{70}-butyric acid methyl ester ($PC_{71}BM$) in a 1:1.5 ratio (w/w) exhibited the best power conversion efficiency (PCE), at 3.26 %.

Introduction

Organic photovoltaics (OPVs) are a promising source of renewable energy for the future. Currently, OPVs are based on two types of electron donor materials: polymers and small molecules.[1] Organic solar cells based on bulk heterojunction (BHJ-OPV) configurations have attracted considerable interest due to their easy fabrication, relatively low cost and their flexibility.[1b,2]

Over the last few years, a significant increase in the power conversion efficiencies (PCE), exceeding 10%, has been achieved by devices based on blends of polymer donors and $PC_{71}BM$ as the acceptor.[3] On the other hand, small molecule based OPVs (SM-OPVs) have achieved PCEs as high as 9.3%.[4] Small molecule donors offer several advantages over polymeric materials such as: easy purification, well-defined molar masses and molecular structures, high solubility and good batch to batch reproducibility.[1b,5]

Donor–acceptor (D–A) alternating small molecules use electron-deficient heterocycles, such as BT,[6] donor moieties such as carbazole,[7] and alkyl-rhodanines[8] as end groups, in order to achieve high efficiencies. To date, small molecules based on carbazole units for BHJ solar cells have not been extensively explored.

In general, OPVs exhibit photoexcited states that are not spatially separated electron-hole pairs but short-lived bound excitons. OPV morphologies are crucial for optimal device performances since the photo-generated charge carriers need to be efficiently transported from the active layer to the electrodes.

SM-OPVs have typically been plagued by low fill factors (FFs), poor film quality and less than optimal-morphologies.[8a] Most small molecule donors possess conjugated linear structures and exhibit better absorption properties and efficiencies.[8b]

The highest published PCEs for solution-processed SM based BHJ-OPVs were obtained by careful molecular design to control the structures and the nanoscale phase separation morphologies.[2a–2c,4] In order to achieve this, molecular designs must address many factors simultaneously, including the nature of the chromophores for high absorption coefficients across the solar spectrum, proper crystallization properties of the donor materials and their morphological compatibility with those of the acceptors. The most widely used methods for controlling the morphology of the active layers in BHJ-SCs are thermal annealing[8e,9] and solvent annealing.[10]

Herein, we report the syntheses, optoelectronic and photovoltaic properties of two new conjugated small molecules, **ECTBT** and **ECBT**, see Scheme 1. The electron-withdrawing building block, benzothiadiazole, was introduced to decrease the HOMO level and to extend the absorption of the D–A band. Carbazole units were introduced as the donor building blocks and 3-octylrhodanine as the electron-withdrawing end-groups, see Scheme 1.

[a] Department of Chemistry, University of Texas at El Paso, 500 W. University Ave., El Paso, TX 79968, USA
E-mail: echegoyen@utep.edu
http://www.science.utep.edu/echegoyen/
[b] Department of Materials Science, University of Texas at El Paso, 500 W. University Ave., El Paso, TX 79968, USA

Supporting information for this article is available on the WWW under http://dx.doi.org/10.1002/ejoc.201500552.

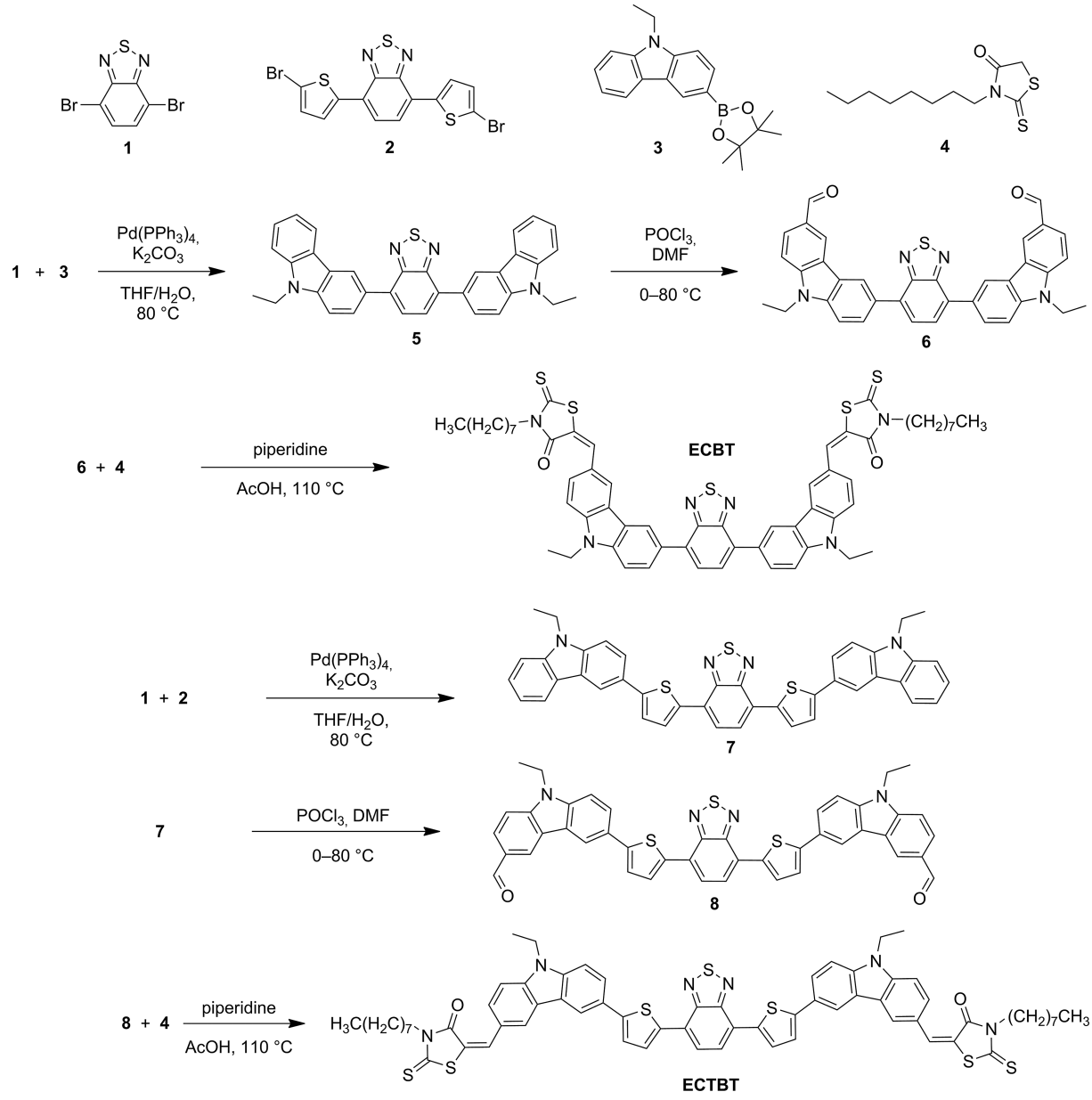

Scheme 1. Syntheses of **ECBT** and **ECTBT**.

Results and Discussion

Synthesis and Thermal Properties

Solvents and reagents were obtained from commercial sources (Rieke Metals Inc., Nano-C Inc., Aldrich and Fisher) and were used as received. Tetrahydrofuran (THF) was dried with sodium/benzophenone and distilled prior to use. The synthetic steps followed to prepare **ECTBT** and **ECBT** are shown in Scheme 1. 4,7-dibromo-2,1,3-benzothiadiazole (**1**),[11] 4,7-Bis(2-bromo-5-thienyl)-2,1,3-benzothiadiazole (**2**),[12] (9-ethyl-9*H*-carbazol-3-yl)boronic acid pinacol ester (**3**),[13] and *N*-octylrhodanine (**4**),[14] were synthesized according to reported procedures.

Compound **5** was synthesized by a Suzuki coupling of **1** and **3**, then formylated using $POCl_3$ in DMF to yield **6** and finally a Knoevenagel condensation in acetic acid and piperidine was performed to afford compound **ECBT**. The same approach was followed for the synthesis of **ECTBT**. The thermal properties of the compounds were determined using thermal gravimetric analysis (TGA) under a nitrogen atmosphere at a heating rate of 5 °C/min up to 500 °C. Both **ECTBT** and **ECTB** showed good thermal stability, indicating that they are suitable for BHJ-SCs fabrication having onset decomposition temperatures (T_d, 5% weight loss) of 350–400 °C.

Optical Properties

The optical properties in solution and in the solid state were measured by UV/Vis absorption spectroscopy as

Table 1. UV/Vis absorption, optical band gap, and HOMO and LUMO levels of small molecules.

SM	Solution[a] λ_{max} [nm]	Solid film[b] λ_{max} [nm]	Energy levels E^{ox}_{onset}/HOMO[c] [eV]	E^{red}_{onset}/LUMO[d] [eV]	Band gaps Eg[e] [eV]	*Eg[f] [eV]
ECBT	301, 360, 453	306, 367, 456	0.52/–5.32	–1.80/–3.00	2.32	2.25
ECTBT	265, 300, 358, 455	365, 554	0.25/–5.05	–1.64/–3.16	1.89	1.63

[a] Absorption spectra measured in chloroform. [b] Spin-coated film from chloroform solution onto a glass surface. [c] E_{HOMO} = –[$(E_{onset})^{ox}$ + 4.8]eV. [d] {E_{LUMO} = –[$(E_{onset})^{red}$ + 4.8]eV}. [e] Electrochemical band gap: $Eg = E_{ox/peak} - E_{red/peak}$. [f] Calculated from the absorption spectra: $Eg = 1240/(\lambda_{onset})_{film}$.

shown in Figure 1. Films were prepared on glass slides by spin-coating from chloroform solutions at room temperature. **ECBT** in solution shows absorption bands in the range between 265–520 nm, with three absorption maxima at 301, 360 and 453 nm, while **ECTBT** shows absorption bands in the range between 265–620 nm, with four absorption maxima at 265, 300, 358 and 455 nm. Peaks around 300 nm are attributed to π–π* transitions of the carbazole moiety, while peaks around 550 nm are attributed to the intramolecular charge-transfer bands (ICT) between the donor and acceptor units.[15] The optical band gaps (E_g^{opt}) for **ECBT** and **ECTBT** were calculated from their absorption onsets at 550 and 760 nm respectively, and the values are presented in Table 1.

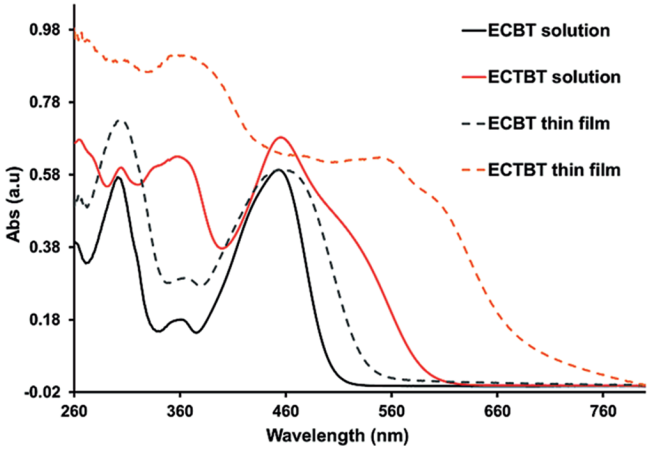

Figure 1. UV/Vis absorption spectra of **ECBT** and **ECTBT** in chloroform solutions and solid state (thin film).

Electrochemical Properties

Cyclic voltammetry (CV) was used to study the electrochemical properties of **ECTB** and **ECTBT**. Figure 2 shows the cyclic voltammograms of the two electron donor compounds, and the electrochemical data are presented in Table 1. In the anodic scan, the two compounds show a first irreversible oxidation wave at +0.52 V for **ECBT** and +0.25 V for **ECTBT** (vs. Fc/Fc^+). The easier oxidation of **ECTBT** (by 0.27 V) is attributed to the presence of the thiophene moieties next to the benzothiadiazole core. Two irreversible reductions were observed in the cathodic scan at –1.8 and –2.0 V for **ECBT** and at –1.64 and –1.8 V for **ECTBT**.

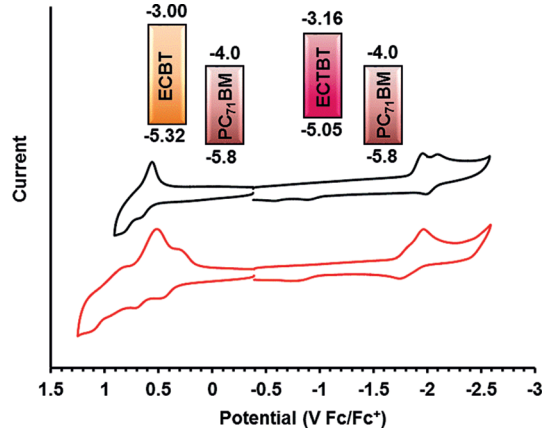

Figure 2. Cyclic voltammograms of **ECBT** and **ECTBT** in *o*-DCB vs. Fc/Fc^+ and energy-level diagrams.

The HOMO and LUMO levels were calculated from the electrochemical oxidation and reduction potentials according to the empirical formula {E_{HOMO} = –[$(E_{onset})^{ox}$ + 4.8]eV} and {E_{LUMO} = –[$(E_{onset})^{red}$ + 4.8]eV} respectively, see Table 1. The electrochemical band gaps, 2.32 eV for **ECBT** and 1.89 eV for **ECTBT** match well the $PC_{71}BM$ values (–5.87 and –3.91 eV),[16] for efficient exciton dissociation and for favorable electron transfer processes to occur between the donor and the acceptor in BHJ-SCs.[17]

Photovoltaic Properties

The photovoltaic properties of **ECBT** and **ECTBT** were investigated by fabricating BHJ devices from an *ortho*-dichlorobenzene (*o*-DCB) solution with an active layer thickness of ca. 80 nm, and a device structure consisting of indium tin oxide (ITO)/poly(3,4-ethylenedioxythiophene): polystyrenesulfonate (PEDOT:PSS)/small molecule: $PC_{71}BM$/Al. Different small molecule:$PC_{71}BM$ blend ratios were investigated. We found that a 1:1.5 ratio for **ECTBT** and a 1:3 ratio for **ECBT** (weight ratios) yielded the maximum PCEs. The values measured were: 3.26% PCE, with a short circuit current (I_{sc}) of 10.18 mA/cm^2, an open circuit voltage (V_{oc}) of 0.78 V, a fill factor (FF) of 49.4% for **ECTBT** and a PCE of 1.45%, with a I_{sc} of 5.40 mA/cm^2, a V_{oc} of 0.74 V, and a FF of 36.2% for **ECBT**.

The optimized devices based on the **ECTBT** and **ECTB** exhibit different V_{oc} values, which correlates well with the energy difference between the HOMO of the donor and the LUMO of the acceptor. **ECBT** (no thiophene spacers) has

a lower V_{oc} (0.74 V) than that of **ECTBT** (0.78 V); unexpectedly the value of the HOMO level of **ECBT** is lower than that of **ECTBT**. As expected, **ECTBT** has a lower band gap than that of **ECBT**. The higher I_{sc} value observed for **ECTBT** can be attributed to the more extended conjugation provided by the thiophene groups,[18] to form an extended A–D–A backbone structure. The device parameters of the cells are presented in Table 2 and the current density-voltage (*I–V*) characteristics of the optimized devices are presented in Figure 3.

Table 2. Photovoltaic properties of **ECBT** and **ECTBT**.

SM	Ratio	Area [mm^2]	V_{oc}[a] [V]	I_{sc} [a] [mA/cm^2]	FF[a] [%]	PCE[a] [%]
ECBT	(1:3)	4	0.740	5.40	36.2	1.45
ECBT	(1:2)	4	0.721	4.37	34.8	1.13
ECTBT	(1:1.3)	4	0.770	9.98	49.6	3.19
ECTBT	(1:1.5)	4	0.780	10.18	49.4	2.26
ECTBT	(1:2)	4	0.817	10.37	47.8	2.30

[a] Average value from eight devices.

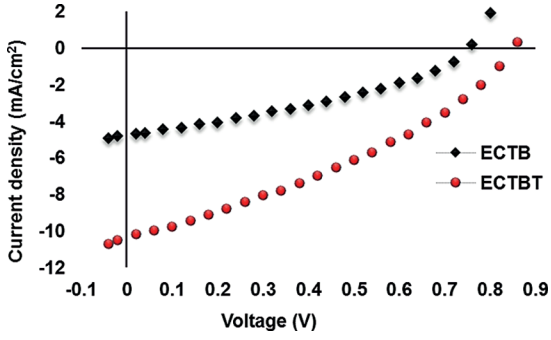

Figure 3. *I–V* curves of BHJ solar cell devices of **ECBT** and **ECTBT**.

Morphologies of the Active Layers

The surface morphologies of the blend films of SMs/$PC_{71}BM$ spin-coated from *o*-DCB solutions were studied using non-contact mode atomic force microscopy (AFM). Figure 4 (a, b) contain the AFM images of the SMs/$PC_{71}BM$ blend films showing the best photovoltaic performance at 200 nm. The films show good phase separation and elongated and ordered donor/acceptor domains for **ECTBT** (Figure 4, b), while larger and less defined domains were observed for the **ECBT** containing devices (Figure 4, a). Due to the large domains present in the **ECBT** active layers, excitons are less likely to reach the D–A interfaces, leading to a decrease in the I_{sc} values. On the basis of the AFM observations, the two small molecules exhibited very different miscibilities and phase separations.

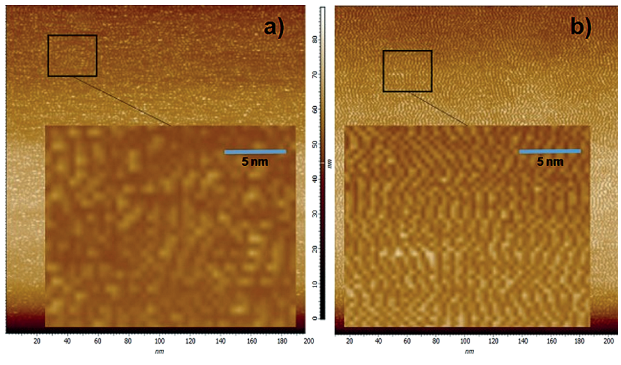

Figure 4. Morphology of SM-OPV active layers at 200 nm × 200 nm resolution a) **ECBT**, b) **ECTBT**.

Although the overall PCE decreased upon increasing the acceptor ratio of ECTBT:$PC_{71}BM$ from 1:1.5 to 1:2.0 (w/w), it increased both the I_{sc} and V_{oc} values, while decreasing the FF value, reflecting the influence of the morphology.[19] On the other hand, when the acceptor ratio of ECBT:$PC_{71}BM$ was increased from 1:2.0 to 1:3.0 all of the performance parameters (I_{sc}, V_{oc}, FF and PCE) decreased (Table 2).

Conclusions

Two new π-conjugated electron-donors **ECBT** and **ECTBT** having an A-D-A architectures based on carbazole as the central donating moieties, BT as the acceptor building block and octylrhodanine as the end groups were investigated. The thiophene π-conjugated spacers between the BT and the carbazole have a pronounced effects on both the optical and electrical properties, giving **ECTBT** a (red-shifted) broad absorption range and an expected low band-gap value. The AFM images of **ECTBT** show continuous and well defined domains, which lead to optimized carrier transport and to higher I_{sc} values and thus to much pronounced higher PCEs.

Experimental Section

Measurements and Instruments: NMR spectra were recorded using a JEOL 600 MHz spectrometer. MALDI-TOF mass spectra were obtained using a Bruker Microflex LRF mass spectrometer. The UV/Vis-NIR spectra were recorded on a Cary 5000 UV/Vis-NIR spectrophotometer. Cyclic voltammetric experiments were done using a one compartment cell and a BAS 100B potentiostat in solutions of *o*-DCB containing 0.05 M nBu_4NPF_6. A 2 mm diameter glassy carbon disk was used as the working electrode, a platinum wire as the counter electrode, and a silver wire as the pseudoreference electrode. Ferrocene was added to the solution at the end of each experiment as an internal potential standard. TGA measurements were performed on a Mettler Toledo TGA/DSC 1 thermogravimetric analyzer. The AFM measurements of the surface morphologies of the samples were obtained on a ND-MDT NTEGRA instrument using the tapping mode.

Fabrication and Characterization: Solar cells were fabricated on ITO-coated glass substrates with a resistivity of 10 Ω/cm^2 and thicknesses of approximately 200 nm. Prior to fabrication, the substrates were cleaned using detergent, deionized water, isopropyl alcohol and acetone, then they were treated in an UV-ozone oven for 30 min. PEDOT:PSS (Clevious P VP Al 4083) was spun-cast at 5000 rpm for 30 s after passing the solution through a 0.22 μm PDVP filter, and annealed in air at 150 °C for 15 min. Solutions of the active layer materials were stirred at 80 °C for 12 h, followed

by spin-casting at 550 rpm for 60 s and 2500 rpm for 2 s after passing the solution through a 0.22 μm PTFE filter to afford about 80-nm-thick active layers. Devices were then transferred to a N_2-filled glove box and additional annealing was performed at 150 °C for 10 min. immediately after they were loaded into a vacuum deposition chamber (background pressure about 4.0×10^{-6} Torr) where a 100-nm-thick aluminum cathode was deposited. The top aluminum electrodes were encapsulated with a UV-curable epoxy resin and a glass slide before testing. Each device had four cells with an average area of 0.04 cm^2. *I–V* characteristics of the devices in the dark and under illumination were recorded on a Photo Emission Tech SS100 Solar Simulator at 100 mW/cm^2 in air.

Synthetic Procedures: Compound **5**. In a 100 mL two-neck round-bottom flask, compounds **1** (145.9 mg, 0.5 mmol) and **3** (321.19 mg, 1.0 mmol) were dissolved in THF/H_2O (20:5 mL) and potassium carbonate (137.91 mg, 1.0 mmol) was then added. The resulting mixture was degassed for 10 min before and after the addition of $Pd(PPh_3)_4$ (11.6 mg, 0.01 mmol). The reaction mixture was heated and stirred at 90 °C under a nitrogen atmosphere for 24 h. The mixture was poured on water (100 mL) and extracted with CH_2Cl_2 (20 mL × 3 times), and the combined organic layers were dried with anhydrous $MgSO_4$. The solvent was removed under reduced pressure and the crude was purified by column chromatography on silica gel using CS_2/$CHCl_3$ (9:1) as eluent to afford **5** as a yellow solid (85%). ^{1}H NMR ($CDCl_3$, 600 MHz): δ = 8.71 (d, *J* = 1.6 Hz, 2 H), 8.21 (d, *J* = 7.7 Hz, 2 H), 8.15 (dd, *J* = 8.4, 1.7 Hz, 2 H), 7.92 (s, 2 H), 7.59 (d, *J* = 8.4 Hz, 2 H), 7.51 (t, *J* = 7.6 Hz, 2 H), 7.46 (d, *J* = 8.2 Hz, 2 H), 7.28 (t, *J* = 6.9 Hz, 2 H), 4.45 (q, *J* = 7.2 Hz, 4 H), 1.49 (t, *J* = 7.3 Hz, 6 H) ppm. ^{13}C NMR ($CDCl_3$, 150 MHz): δ = 154.8, 140.5, 140.0, 133.5, 128.7, 128.1, 127.3, 125.8, 123.4, 123.3, 121.4, 120.8, 119.2, 108.7, 108.6, 37.8, 14.0 ppm. MS (MALDI-TOF): calcd. for $C_{34}H_{26}N_4S$ 522.19, found 522.16 [M^+].

Compound 6: In a 100 mL two-neck round-bottom flask, compound **5** (302 mg, 0.58 mmol) and 20 mL of dry of DMF were added. The mixture was stirred at 0 °C for 10 min, then $POCl_3$ (0.54 mL, 5.83 mmol) was added dropwise, warmed to room temperature (after 20 min) and stirred for 30 min, and then heated at 80 °C overnight. The mixture was poured on water (100 mL) and extracted with CH_2Cl_2 (20 mL × 3 times), and the combined organic layers were dried with anhydrous $MgSO_4$. The solvent was removed under reduced pressure and the crude was purified by column chromatography on silica gel using CS_2/$CHCl_3$ (9:1) as eluent to afford **6** as an orange solid (82%). ^{1}H NMR ($CDCl_3$, 600 MHz): δ = 10.13 (s, 2 H), 8.81 (d, *J* = 1.6 Hz, 2 H), 8.74 (d, *J* = 1.4 Hz, 2 H), 8.21 (dd, *J* = 8.4, 1.7 Hz, 2 H), 8.06 (dd, *J* = 8.5, 1.5 Hz, 2 H), 7.95 (s, 2 H), 7.65 (d, *J* = 8.5 Hz, 2 H), 7.54 (d, *J* = 8.5 Hz, 2 H), 4.49 (q, *J* = 7.3 Hz, 4 H), 1.54 (t, *J* = 7.4 Hz, 6 H) ppm. ^{13}C NMR ($CDCl_3$, 150 MHz): δ = 191.9, 154.6, 144.1, 140.8, 133.3, 130.1, 128.9, 128.3, 128.2, 127.6, 124.3, 123.6, 123.5, 121.9, 109.4, 109.1, 38.3, 14.0 ppm. MS (MALDI-TOF): calcd. for $C_{36}H_{26}N_4O_2S$ 578.18, found 578.19 [M^+].

Compound ECBT: A mixture of a compound **6** (200 mg, 0.26 mmol) and piperidine (3 drops), were stirred in acetic acid (15 mL) at 110 °C for 16 h. After cooling the mixture, it was dried under vacuum. The crude was purified by column chromatography on silica gel using $CHCl_3$:*n*-C_6H_{14} (1:1) as eluent to afford a red solid (76%). ^{1}H NMR ($CDCl_3$, 600 MHz): δ = 8.71 (d, *J* = 1.7 Hz, 2 H), 8.33 (d, *J* = 1.7 Hz, 2 H), 8.23 (dd, *J* = 8.4, 1.7 Hz, 2 H), 7.97 (s, 2 H), 7.96 (s, 2 H), 7.64 (dd, *J* = 8.7, 1.7 Hz, 2 H), 7.62 (d, *J* = 8.5 Hz, 2 H), 7.51 (d, *J* = 8.6 Hz, 2 H), 4.45 (q, *J* = 7.2 Hz, 4 H), 4.16–4.10 (m, 4 H), 1.76–1.69 (m, *J* = 15.1, 7.7 Hz, 4 H), 1.52 (t, *J* = 7.3 Hz, 6 H), 1.40–1.25 (m, 20 H), 0.87 (t, *J* = 7.1 Hz, 6 H) ppm. ^{13}C NMR ($CDCl_3$, 150 MHz): δ = 193.7, 168.2, 154.7, 141.7 (× 2), 140.6, 134.9, 133.3, 130.1, 128.9, 128.4, 126.9, 124.8, 124.2, 123.2, 121.7, 119.2, 109.7, 109.3, 31.9, 29.3, 29.2, 27.1, 26.9, 22.7 (× 3), 14.2, 14.0 ppm. MS (MALDI-TOF): calcd. for $C_{58}H_{60}N_6O_2S_5$ 1032.34, found 1032.41 [M^+].

Compound 7: Compound **7** was synthesized by the same procedure as that used to prepare compound **5**, to afford an orange solid (65%). ^{1}H NMR ($CDCl_3$, 600 MHz): δ = 8.46 (d, *J* = 1.5 Hz, 2 H), 8.21 (d, *J* = 7.7 Hz, 2 H), 8.18 (d, *J* = 4.0 Hz, 2 H), 7.94 (s, 2 H), 7.87 (dd, *J* = 8.6, 1.8 Hz, 2 H), 7.53 (t, *J* = 7.1 Hz, 2 H), 7.48 (d, *J* = 4.0 Hz, 2 H), 7.46 (d, *J* = 8.5 Hz, 2 H), 7.30 (t, *J* = 7.9 Hz, 2 H), 4.42 (q, *J* = 7.2 Hz, 4 H), 1.49 (t, *J* = 7.2 Hz, 6 H) ppm. ^{13}C NMR ($CDCl_3$, 150 MHz): δ = 151.8, 139.8, 137.5, 130.2, 128.7, 127.1, 126.1, 125.4, 125.2, 124.1, 124.2, 123.0, 122.9, 120.7, 119.2, 117.9, 117.5, 108.8, 108.7, 37.9, 13.9 ppm. MS (MALDI-TOF): calcd. for $C_{42}H_{30}N_4S_3$ 686.16, found 686.23 [M^+].

Compound 8: Compound **8** was synthesized using the same procedure used to prepare compound **6**, to afford a dark orange solid (70%). ^{1}H NMR ($CDCl_3$, 600 MHz): δ = 10.11 (s, 2 H), 8.64 (s, 2 H), 8.44 (s, 2 H), 8.13 (dd, *J* = 3.7, 2.4 Hz, 2 H), 8.03 (dd, *J* = 8.4, 1.5 Hz, 2 H), 7.88 (d, *J* = 10.6 Hz, 4 H), 7.49–7.43 (m, 6 H), 4.40 (q, *J* = 7.3 Hz, 4 H), 1.49 (t, *J* = 7.3 Hz, 6 H) ppm. ^{13}C NMR ($CDCl_3$, 150 MHz): δ = 191.8, 152.7, 146.4, 144.1, 140.7, 130.4, 130.2, 128.9, 128.7, 127.5, 127.4, 126.0, 125.7, 125.2, 125.1, 124.4, 123.5, 118.1, 109.6, 109.1, 38.0, 13.9 ppm. MS (MALDI-TOF): calcd. for $C_{44}H_{30}N_4O_2S_3$ 742.15, found 742.32 [M^+].

Compound ECTBT: Compound **ECTBT** was synthesized using the same procedure used to prepare compound **ECBT**, to afford a dark red solid (80%). ^{1}H NMR ($CDCl_3$, 600 MHz): δ = 8.45 (s, 2 H), 8.28 (s, 2 H), 8.21 (d, *J* = 7.7 Hz, 2 H), 7.96–7.92 (m, 4 H), 7.61 (dd, *J* = 17.3, 8.6 Hz, 4 H), 7.54–7.49 (m, 6 H), 4.42 (q, *J* = 7.5 Hz, 4 H), 4.12 (q, *J* = 7.1 Hz, 4 H), 1.71–1.77 (m, 4 H), 1.50 (t, *J* = 8.2 Hz, 6 H), 1.36–1.25 (m, 20 H), 0.88 (t, *J* = 8.1 Hz, 6 H) ppm. ^{13}C NMR ($CDCl_3$, 150 MHz): δ = 194.2, 167.9, 165.5, 156.6, 152.6, 151.3, 139.8, 139.7, 136.5, 134.2, 129.2, 127.3, 126.8, 126.5, 125.9, 123.8, 123.5, 120.8, 119.6, 119.3 (× 2), 109.1, 108.9, 31.8, 29.8 (× 2), 29.2, 26.9, 22.7 (× 3), 14.2 (× 2) ppm. MS (MALDI-TOF): calcd. for $C_{66}H_{64}N_6O_2S_7$ 1196.31, found 1196.54 [M^+].

Acknowledgments

The authors thank the US National Science Foundation (NSF), grant numbers CHE-1408865, and DMR-1205302 (PREM program) and the Robert A. Welch Foundation for an endowed chair to L. E., grant number AH-0033, for their generous support.

[1] a) B. C. Thompson, J. M. J. Fréchet, *Angew. Chem. Int. Ed.* **2007**, *47*, 58–77; *Angew. Chem.* **2007**, *120*, 62–82; b) A. Mishra, P. Bäuerle, *Angew. Chem. Int. Ed.* **2012**, *51*, 2020–2067; *Angew. Chem.* **2012**, *124*, 2060–2109.

[2] a) G. Li, V. Shrotriya, Y. Yao, J. Huang, Y. Yang, *J. Mater. Chem.* **2007**, *17*, 3126–3140; b) C. J. Brabec, N. S. Sariciftci, J. C. Hummelen, *Adv. Funct. Mater.* **2001**, *11*, 15–26; c) S. Loser, C. J. Bruns, H. Miyauchi, R. P. Ortiz, A. Facchetti, S. I. Stupp, T. J. Marks, *J. Am. Chem. Soc.* **2011**, *133*, 8142–8145; d) F. C. Krebs, S. A. Gevorgyan, J. Alstrup, *J. Mater. Chem.* **2009**, *19*, 5442–5451; e) B. Zhao, Z. He, X. Cheng, D. Qin, M. Yun, M. Wang, X. Huang, J. Wu, H. Wu, Y. Cao, *J. Mater. Chem. C* **2014**, *2*, 5077–5082.

[3] a) J. You, L. Dou, K. Yoshimura, T. Kato, K. Ohya, T. Moriarty, K. Emery, C.-C. Chen, J. Gao, G. Li, Y. Yang, *Nat. Commun.* **2013**, *4*, 1446; b) H. Zhou, Y. Zhang, C.-K. Mai, S. D.

Collins, G. C. Bazan, T.-Q. Nguyen, A. J. Heeger, *Adv. Mater.* **2015**, 27, 1767–1773.
[4] K. Sun, Z. Xiao, S. Lu, W. Zajaczkowski, W. Pisula, E. Hanssen, J. M. White, R. M. Williamson, J. Subbiah, J. Ouyang, A. B. Holmes, W. W. H. Wong, D. J. Jones, *Nat. Commun.* **2015**, *6*.
[5] a) Y. Lin, Y. Li, X. Zhan, *Chem. Soc. Rev.* **2012**, *41*, 4245–4272; b) B. Walker, C. Kim, T.-Q. Nguyen, *Chem. Mater.* **2011**, *23*, 470–482.
[6] a) T. S. van der Poll, J. A. Love, T.-Q. Nguyen, G. C. Bazan, *Adv. Mater.* **2012**, *24*, 3646–3649; b) H.-I. Lu, C.-W. Lu, Y.-C. Lee, H.-W. Lin, L.-Y. Lin, F. Lin, J.-H. Chang, C.-I. Wu, K.-T. Wong, *Chem. Mater.* **2014**, *26*, 4361–4367; c) W. Yong, M. Zhang, X. Xin, Z. Li, Y. Wu, X. Guo, Z. Yang, J. Hou, *J. Mater. Chem. A* **2013**, *1*, 14214–14220; d) V. Gupta, A. K. K. Kyaw, D. H. Wang, S. Chand, G. C. Bazan, A. J. Heeger, *Sci. Rep.* **2013**, *3*; e) H. Shang, H. Fan, Y. Liu, W. Hu, Y. Li, X. Zhan, *Adv. Mater.* **2011**, *23*, 1554–1557; f) Y.-H. Chen, L.-Y. Lin, C.-W. Lu, F. Lin, Z.-Y. Huang, H.-W. Lin, P.-H. Wang, Y.-H. Liu, K.-T. Wong, J. Wen, D. J. Miller, S. B. Darling, *J. Am. Chem. Soc.* **2012**, *134*, 13616–13623.
[7] a) J. Lu, P. F. Xia, P. K. Lo, Y. Tao, M. S. Wong, *Chem. Mater.* **2006**, *18*, 6194–6203; b) J.-F. Morin, M. Leclerc, D. Adès, A. Siove, *Macromol. Rapid Commun.* **2005**, *26*, 761–778.
[8] a) Z. Li, G. He, X. Wan, Y. Liu, J. Zhou, G. Long, Y. Zuo, M. Zhang, Y. Chen, *Adv. Energy Mater.* **2012**, *2*, 74–77; b) Y. Liu, C.-C. Chen, Z. Hong, J. Gao, Y. Yang, H. Zhou, L. Dou, G. Li, Y. Yang, *Sci. Rep.* **2013**, *3*; c) J. Zhou, Y. Zuo, X. Wan, G. Long, Q. Zhang, W. Ni, Y. Liu, Z. Li, G. He, C. Li, B. Kan, M. Li, Y. Chen, *J. Am. Chem. Soc.* **2013**, *135*, 8484–8487; d) J. Zhou, X. Wan, Y. Liu, Y. Zuo, Z. Li, G. He, G. Long, W. Ni, C. Li, X. Su, Y. Chen, *J. Am. Chem. Soc.* **2012**, *134*, 16345–16351; e) Z. Yi, W. Ni, Q. Zhang, M. Li, B. Kan, X. Wan, Y. Chen, *J. Mater. Chem. C* **2014**, *2*, 7247–7255.
[9] W. Ma, C. Yang, X. Gong, K. Lee, A. J. Heeger, *Adv. Funct. Mater.* **2005**, *15*, 1617–1622.
[10] a) G. Li, V. Shrotriya, J. Huang, Y. Yao, T. Moriarty, K. Emery, Y. Yang, *Nat. Mater.* **2005**, *4*, 864–868; b) C. Sinturel, M. Vayer, M. Morris, M. A. Hillmyer, *Macromolecules* **2013**, *46*, 5399–5415.
[11] B. A. DaSilveira Neto, A. S. A. Lopes, G. Ebeling, R. S. Gonçalves, V. E. U. Costa, F. H. Quina, J. Dupont, *Tetrahedron* **2005**, *61*, 10975–10982.
[12] I. Palamà, F. Di Maria, I. Viola, E. Fabiano, G. Gigli, C. Bettini, G. Barbarella, *J. Am. Chem. Soc.* **2011**, *133*, 17777–17785.
[13] S. H. Kim, I. Cho, M. K. Sim, S. Park, S. Y. Park, *J. Mater. Chem.* **2011**, *21*, 9139–9148.
[14] S. Wang, Y. Zhao, G. Zhang, Y. Lv, N. Zhang, P. Gong, *Eur. J. Med. Chem.* **2011**, *46*, 3509–3518.
[15] a) J. Kim, M. H. Yun, P. Anant, S. Cho, J. Jacob, J. Y. Kim, C. Yang, *Chem. Eur. J.* **2011**, *17*, 14681–14688; b) L. Huo, X. Guo, Y. Li, J. Hou, *Chem. Commun.* **2011**, *47*, 8850–8852.
[16] Y. He, Y. Li, *Phys. Chem. Chem. Phys.* **2011**, *13*, 1970–1983.
[17] M. C. Scharber, D. Mühlbacher, M. Koppe, P. Denk, C. Waldauf, A. J. Heeger, C. J. Brabec, *Adv. Mater.* **2006**, *18*, 789–794.
[18] R. S. Kularatne, P. Sista, H. Q. Nguyen, M. P. Bhatt, M. C. Biewer, M. C. Stefan, *Macromolecules* **2012**, *45*, 7855–7862.
[19] Y. Liu, X. Wan, B. Yin, J. Zhou, G. Long, S. Yin, Y. Chen, *J. Mater. Chem.* **2010**, *20*, 2464–2468.

Received: April 29, 2015
Published Online: June 5, 2015

